



Continuous manganese(II) ions removal from aqueous solutions using rice husk ash-packed column reactor

Ningning Li^a, Jiaying Zhao^b, Zhao Jiang^b, Bo Cao^b, Yan Lu^b, Dexin Shan^b, Ying Zhang^{b,*}

^aSchool of College of Forestry, Northeast Forestry University, Harbin 150040, PR China, email: 82624907@163.com

^bSchool of Resource and Environment, Northeast Agricultural University, Harbin 150030, PR China, emails: zhaojianan_2012@163.com (J. Zhao), jiangzhao_0828@163.com (Z. Jiang), cb870912@hotmail.com (B. Cao), 986509351@qq.com (Y. Lu), shanshuo0219@126.com (D. Shan), Tel. +86 0451 55190993; Fax: +86 451 55191170; email: zhangyinghr@hotmail.com (Y. Zhang)

Received 9 March 2015; Accepted 18 November 2015

ABSTRACT

This study was conducted to analyse the biosorption of manganese(II) from aqueous solutions by rice husk ash (RHA) in a continuous packed column reactor. Different column parameters were used, such as influent Mn(II) concentration, bed height and flow rate. The results showed that the equilibrium adsorption (mg g^{-1}) has increased after increasing the influent Mn(II) concentration but decreased when increasing the flow rate and the bed height. When the influent Mn(II) concentration was expanded from 5 to 20 mg l^{-1} at a fixed bed height and flow rate, then Mn(II) uptake also expanded from 2.73 to 4.76 mg g^{-1} . Similarly, by increasing the bed height from 7.5 to 22.5 cm and flow rate from 5 to 15 ml min^{-1} , the adsorption capacity of Mn(II) decreased from 7.57 to 2.97 mg g^{-1} and 3.61 to 1.90 mg g^{-1} , respectively. In addition, several empirical models such as Adams–Bohart, Wolborska, Thomas and Yoon–Nelson models were used in this study to investigate the breakthrough curves in a simple way. The best fitting was obtained with Adams–Bohart and Wolborska models which showed high degree of fitting ($r^2 \geq 0.82$). So Bohart–Adams and Wolborska models were the most suitable to estimate breakthrough curves obtained under varying experimental conditions.

Keywords: Biosorption; Packed column reactor; Rice husk ash; Manganese(II) ions; Breakthrough curve

1. Introduction

In recent era, surging industrial activities caused more environmental problems, such as ecosystems degradation leading to the accumulation of pollutants just like heavy metals [1]. Heavy metals are very toxic water pollutants and can cause damage to humans by entering in food pyramid [2]. Moreover, large number

of industrial emissions contains heavy metals, such as nonferrous metal smelting, mining operations, tanneries, chemical materials and chemical products manufacturing, which may cause fresh and marine water pollution [3,4]. Among various heavy metals, the Mn (II) ions were mainly existed in ground water and some other water which were collected from the bottom anoxic zones of reservoirs [5]. Though Mn(II) in surface waters was a trace element, the accumulation

*Corresponding author.

of manganese ions was not only toxic to fish and humans but also affect the drinking water quality seriously [6,7]. For example, the oxide which was formed and deposited in drinking water pipeline caused high concentrations of Mn(II) in drinking water than the standards, which resulted in discolouration and unpleasant metallic taste of water [8,9]. According to US Environmental Protection Agency (EPA), maximum contaminant level of Mn(II) in drinking water was 0.1 mg l^{-1} [10]. Nowadays, many techniques such as filtration, precipitation, ion exchange, adsorption, oxide reduction and reverse osmosis are being used to remove different heavy metal from water [11]. But the adsorption technique is high efficiency, low cost and user-friendly for the removal of heavy metal. This process seemed to be the most versatile and effective method for removal of heavy metals if coupled with appropriate regeneration steps and available adsorbent. Many studies were carried out on agricultural waste materials such as polymerized onion skin [12], rice husks, maize cobs and sawdust [13], rice bran [14], wheat shell and papaya wood [15] to investigate their effects on binding of heavy metal ions. Rice husk was a kind of high-yield agriculture waste obtained from the rice mills. It was mainly used as a fuel in boiler steam production of various industries. Since RHA was available in plenty and it has very high potential as an adsorbent, the present study has been undertaken to report in the surface characteristics of RHA and the static adsorption characteristics for Cu (II), Fe(II), Mn(II) [16], Hg(II) [17], Pb(II) [18], Cd(II), Ni(II) and Zn(II) [19] ions from aqueous solutions. It needed more consideration to study the dynamic adsorption experiments for practical application. The main objectives of current study was to analyse the adsorption of Mn(II) by RHA from an aqueous solution by a continuous flow reactor. To examine the effects of adsorption parameters such as influent metal concentration, flow rate and adsorbent dosage. In addition, several theoretical models were used to analyse the breakthrough curves.

2. Materials and methods

2.1. Adsorbent preparation from highly active rice husk ash

The rice husk ash (RHA) was collected from Heilongjiang Province Shangzhi surrounding Rice mill. The preparation of highly active RHA consisted of two steps. The first step was at 350°C , volatiles began to burn. From 400 to 500°C , organic matter decomposition and carbonized completely. The second step was under suitable combustion temperature about 530 – 600°C , to carbonize RHA and get the large specific

surface area of RHA, finally meet the requirements to adsorb metal ions.

2.2. Mn(II) adsorption experiments in a packed column

The study was carried out in a Perspex column with an inner diameter of 3.0 cm and a height of 30.0 cm. The metal solution was passed through the column in the downstream flow direction with the help of a miniature peristaltic pump (model BQ50–1 J, China). The flow rate of the inlet was controlled by glass rotameter. The initial concentration of Mn(II) were taken as 5, 10 and 20 mg l^{-1} at a constant bed height 22.5 cm, and flow rate. Experiments were also conducted with bed heights of 7.5, 15 and 22.5 cm, keeping initial Mn(II) concentration of 10 mg l^{-1} and flow rate of 10 ml min^{-1} . Moreover, the effect of flow rates of 5, 10 and 15 ml min^{-1} were observed with the bed height of 22.5 cm and initial Mn(II) concentration of 10 mg l^{-1} at 25°C . In all cases, the initial pH of the solution was adjusted to 5.0 because a preliminary screening showed this value of pH not only could prevent valence change of Mn(II), but also prevent excessive pH to cause the generation of hydroxide precipitate. The BET surface area, total pore volume and the average pore of RHA were showed in Table 1. The effluent was collected at different periods of time (5, 10, 15, 20, 30, 40, 60, 80, 120 min, then sample was taken after every 40 min until adsorption saturation). Mn(II) concentration of the solutions were determined using plasmaoptical emission spectrometry (ICP-OES, PerkinElmer DV5300). Fourier transform infrared (FT-IR) spectrometer (Spectrum one B, Perkin Elmer) was used to analyse spectra recorded at 400 – $4,000 \text{ cm}^{-1}$ which were emitted by each adsorbent prepared as KBr discs. All experimental data were displayed in the form of breakthrough curves.

2.3. BET surface area and pore structure

The surface area and pore structure characterization results of RHA are shown in Table 1. RHA had the large surface area, numerous studies had shown that RHA was a porous material containing a large amount of silicon and had a large specific surface area. The value of BET specific surface area is in the range of 50 – $100 \text{ m}^2 \text{ g}^{-1}$ measured by N_2 adsorption. The specific surface area of RHA is $58.3863 \text{ m}^2 \text{ g}^{-1}$, in the range of 50 and $100 \text{ m}^2 \text{ g}^{-1}$. The total pore volume and the average pore diameter of RHA reached $0.0402 \text{ cm}^3 \text{ g}^{-1}$ and 27.5068 \AA . A large specific surface area and pore structure provide a greater chance of combination between RHA and heavy metal ions.

Table 1
Parameters of pore structure of the RHA

Parameter	BET surface area/(m ² g ⁻¹)	The total pore volume/(cm ³ g ⁻¹)	The average pore diameter/(Å)
RHA	58.3863	0.0402	27.5068

2.4. Experimental data analysis

The breakthrough curves were usually represented by plotting C_t/C_0 vs. the reaction time under various conditions. C_t and C_0 were the Mn(II) concentration (mg l⁻¹) of effluent and influent, respectively.

The total column adsorption capacity, q_{total} (mg) was calculated using Eq. (1) as follows:

$$q_{\text{total}} = \frac{(C_0 - C_t) \times t_{\text{total}} \times Q}{1000} = (C_0 - C_t) \times V_s \quad (1)$$

where t_{total} , Q and V_s are the saturation time of the column (min), flow rate (ml min⁻¹) and the total volume (l) of effluent stored till saturation, respectively. Adsorbed Mn(II) concentration C_{Mn} ($C_{\text{Mn}} = C_0 - C_t$).

Mn(II) adsorption at saturation by per unit weight of the RHA packed in the column, q_s (mg g⁻¹), was calculated using Eq. (2):

$$q_s = \frac{q_{\text{total}}}{M} \quad (2)$$

where M was the total dry weight (g) of RHA packed in the column.

The total amount of Mn(II) ions (M_{total}) supplied to the column till saturation was calculated from Eq. (3):

$$M_{\text{total}} = \frac{C_0 Q t_{\text{total}}}{1000} \quad (3)$$

Total percentage removal (%) of Mn(II) ions was calculated according to Eq. (4):

$$\text{Percentage removal (\%)} = \frac{q_{\text{total}}}{M_{\text{total}}} \times 100 \quad (4)$$

2.5. Theoretical models for the modelling of breakthrough curves

Bohart–Adams, Wolborska, Thomas and Yoon–Nelson models were applied to analyse the breakthrough curves. These models are briefly described below.

2.5.1. The Bohart–Adams model

Bohart and Adams (1920) developed a very simple equation for analysing the chlorine-charcoal transmission curve. This model has been successfully used in predicting breakthrough curves and optimizing the parameters for metal adsorption [20–24]. The basic form of the model is shown by Eq. (5):

$$\frac{C_t}{C_0} = \exp\left(k_{\text{BA}} C_i t - k_{\text{BA}} N_0 \frac{H}{W}\right) \quad (5)$$

where C_0 and C_t were influent metal concentration and effluent metal concentration, respectively, k_{BA} was the kinetic constant (l mg⁻¹ min⁻¹), W was the flow rate (cm min⁻¹), H was the bed height of column (cm) and N_0 was the saturation concentration (mg l⁻¹) of column. The parameters k_{BA} and N_0 of Bohart–Adams model were evaluated by fitting Eq. (1) to the experimental breakthrough curve using the nonlinear regression method.

2.5.2. Wolborska model

Wolborska and Pustelnik (1996) analysed the adsorption of p-nitrophenol on activated carbon and developed a model to describe the breakthrough curves. It can be expressed as Eq. (6):

$$\frac{C_t}{C_0} = \exp\left(\frac{\theta_a C_0 t}{N_0} - \frac{\theta_a H}{W}\right) \quad (6)$$

where θ_a was kinetic diffusion coefficient (h⁻¹). Whenever the parameter $k_{\text{BA}} = \theta_a/N_0$ then the Wolborska and Bohart–Adams model were equivalent.

2.5.3. The Thomas model

The Thomas model was another one frequently used to estimate the adsorptive capacity of metal adsorbent and describe breakthrough curves [23,25,26]. The Thomas model is described by Eq. (7):

$$\frac{C_t}{C_0} = \frac{1}{1 + \exp(k_{\text{Th}} q_0 \frac{M}{F} - k_{\text{Th}} t)} \quad (7)$$

where k_{Th} was the Thomas rate constant ($l\text{ mg}^{-1}\text{ h}^{-1}$), q_0 denoted the equilibrium metal adsorption (mg g^{-1}), C_t and C_0 were effluent metal concentration and influent metal concentration (mg l^{-1}), M was the amount of RHA in fixed bed (g) and F was the flow rate (ml min^{-1}).

2.5.4. The Yoon–Nelson model

The Yoon–Nelson model not only has extremely concise form than other three models, but also requires no detailed data concerning the characters of adsorbate and adsorbent, as well as the parameters of the fixed bed [27]. It expressed through Eq. (8):

$$\frac{C_t}{C_0} = \frac{\exp(k_{YN}t - \tau k_{YN})}{1 + \exp(k_{YN}t - \tau k_{YN})} \quad (8)$$

where k_{YN} was the Yoon–Nelson model rate constant and τ was the time required for 50% adsorbate breakthrough (h).

All models were fitted into the experimental breakthrough curves using nonlinear regression method, and their applicability for evaluation based on r^2 and the standard error of the parameters of these models.

3. Results and discussion

3.1. FT-IR spectra

The FT-IR technique, as an important tool to identify the characteristic of functional groups, can be used to investigate the chemical compositions of the adsorbents material, which are very important for the adsorption of metal ions. The FT-IR spectra of the RHA were shown in Fig. 1. The wave number range of FT-IR spectrum is from 400 to $4,000\text{ cm}^{-1}$. According to Fig. 1, after adsorption of Mn(II), the stretching vibration of bounded hydroxyl group transferred from $3,445.09\text{ cm}^{-1}$ to $3,423.17\text{ cm}^{-1}$, this illustrated the $-\text{OH}$ groups exist in the surface of the RHA occurred chemical reactions with metal ions [28,29]. The peak at $1,096.68\text{ cm}^{-1}$ transferred to $1,094.65\text{ cm}^{-1}$ was attributed to stretching vibration of ether. The peaks observed at 793.43 cm^{-1} can be assigned to the C–H group, and transferred to 787.51 cm^{-1} . These results indicated that the ether and aromatic hydrocarbons functional groups on RHA surface occurred ions exchange with Mn(II). O–Si–O bending vibration transferred from 466.94 cm^{-1} to the 469.67 cm^{-1} after the adsorption of Mn(II). The presence of these functional groups not only proved the main component of RHA is Si, C, O, but also proved these functional

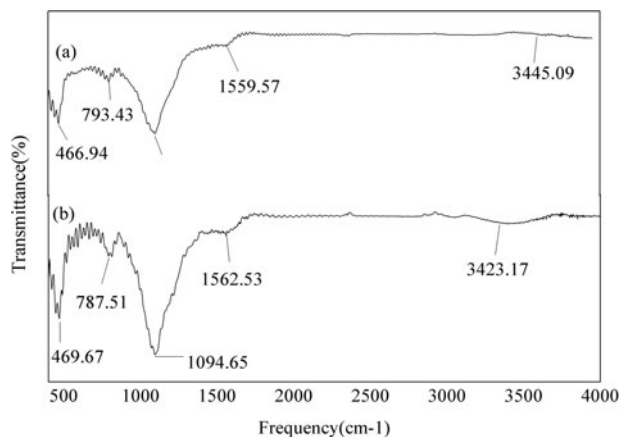


Fig. 1. FT-IR spectrum of RHA before and after adsorption of Mn(II): (a) unloaded RHA and (b) Mn(II)-loaded RHA.

groups may react with the metal ion as complexation [30], which also explained the functional groups onto adsorbent surface played a big role in the heavy metal adsorption process. In addition to the chemical interaction between the RHA and functional groups, the large surface area of RHA also provides a greater chance of combination between RHA and heavy metal ions.

3.2. Breakthrough curves in relation to influent Mn(II) ions concentration

The effect of influent Mn(II) ions concentration (from 5 to 20 mg l^{-1}) on the breakthrough curves using a bed height of 22.5 cm at a constant flow rate of 10 ml min^{-1} are shown in Fig. 2. Table 2 showed that the breakthrough time and saturation time decreased from 14.3 to 4.7 h , 11.9 to 5.2 h , respectively, for the influent Mn(II) ions concentration increased from 5 to 20 mg l^{-1} . These results led to the conclusion that the breakthrough time and saturation time decreased after increasing initial Mn(II) ions concentration. In addition, the breakthrough volume and saturation volume of Mn(II) solution also higher at lower influent concentration of Mn(II) ions than that at a higher Mn(II) ions concentration. In contrast, the sharper breakthrough curves were obtained at higher influent Mn(II) ions concentration than at lower influent Mn(II) ions concentration. This result showed that a high influent concentration saturated the RHA more quickly, and the breakthrough was reached before all the active sites of the adsorbent were occupied by the metal ions [25]. Luo et al. have also found the rise in the inlet metal concentration reduced the treated volume before the rice husk fixed bed adsorption gets

Table 2
Adsorption of Mn(II) ion at various experimental parameters by the RHA-packed column

C_0	H	F	t_b	V_b	t_s	V_s	q_b	q_s	% PR
5	22.5	10	14.3	8.6	19.8	11.9	1.79	2.73	96.59
10	22.5	10	8	4.8	11.3	6.8	1.82	2.97	91.95
20	22.5	10	4.7	2.8	8.7	5.2	2.26	4.76	96.36
10	22.5	5	14.7	4.4	25.7	7.7	3.61	7.01	95.83
10	22.5	15	2.7	2.4	7.3	6.6	1.9	5.89	93.94
10	7.5	10	2	1.2	4.7	2.8	2.87	7.57	94.86
10	15.0	10	3.3	2	6	3.6	2.41	4.84	94.35

Notes: C_0 = influent concentration (mg l^{-1}), F = Flow rate (ml min^{-1}), H = Bed height (cm), t_b = breakthrough time (h), V_b = breakthrough volume (l), t_s = saturation time (h), V_s = saturation volume (l), q_b = adsorption at breakthrough point (mg g^{-1}), q_s = adsorption at saturation point (mg g^{-1}) and % PR = total percentage removal (%) of Mn(II) ions at saturation.

saturated, a high Cu(II) concentration may saturate the rice husk more quickly [31]. Sugashini and Begum observed that the breakthrough time and exhaustion time were occurred slowly at lower influent Cr(VI) ion concentration and also the treated volume of Cr(VI) ions also larger at low influent concentration of Cr(VI) ion [32]. All these results showed that breakthrough time decreased by increasing influent Mn(II) ions concentration. The efficiency of the treatment process to reach the saturation could be measured by the steepness of curve, the steeper the curve, the better adsorption performance. A high influent concentration caused a high driving force for the adsorption process and this might explain why higher adsorption capacities were attained in the column filled with a higher Mn(II) concentration.

3.3. Breakthrough curves in relation to bed height

The breakthrough curves on adsorption of Mn(II) was investigated for various bed height from 7.5 to 22.5 cm at influent Mn(II) ions concentration of 10 mg l^{-1} , flow rate of 10 ml min^{-1} are shown in Fig. 3. Table 2 depicted clearly that the breakthrough time and saturation time were increased from 2.0 to 8.0 h, 4.7 to 11.3 h, respectively, and the bed height was increased from 7.5 to 22.5 cm. The shape and the gradient of the breakthrough curves were changed by altering the bed height, because column had a larger amount of biosorbent and provided a greater number of sites for the binding of metal ions, which resulted longer time for reaching breakthrough and saturation. Therefore, higher bed height could treat larger amount of metal solution. Luo et al. have found an increase in breakthrough time from 3 to 6.6 h by increasing the

adsorbent dosage from 5 to 15 g for an expanding rice husk fixed bed column [31]. Lodeiro et al. have observed the saturation of a protonated Sargassum muticum column in 20, 35 and 56 h, respectively, for 7.4, 13 and 16.6 cm bed height [33]. It was empirical that the breakthrough time and equilibrium time were increased with increase in bed height [34,35]. The slope of the breakthrough curve for larger bed height was lower than that of a smaller bed height. For a greater bed height, especially at lower liquid flow rates, although metal adsorption per unit biomass did not increase, but larger volume of the metal solution could be treated, and a higher percentage of metal ions could be removed.

3.4. Breakthrough curves in relation to flow rate

The flow rate was a very important parameter affecting the breakthrough curves because it determined the contact period of the adsorbate with the adsorbent in the column. Breakthrough curves for the adsorption of Mn(II) by the RHA-packed column in relation to various flow rate from 5 to 15 ml min^{-1} , the influent Mn(II) concentration was kept constant at 10 mg l^{-1} and the bed height was 22.5 cm are given in Fig. 1. The breakthrough time and saturation time decreased from 14.7 to 2.7 h, 25.7 to 7.3 h, respectively, for the flow rate increases from 5 to 15 ml min^{-1} (Table 2). This result demonstrates that the breakthrough and saturation time decreased with increasing influent flow rate at a fixed bed height. The result of a short breakthrough time at high flow rate of metal solution have been previously reported by other researchers [36,37]. For instance, Sugashini and Begum investigated the Cr(VI) removal performance of ozone-treated rice husk carbon-packed bed at flow rate of $5\text{--}25 \text{ ml min}^{-1}$ [38]. They observed that breakthrough time and saturation time were the longest at 5 ml min^{-1} and the shortest at 25 ml min^{-1} . Luo et al. studied that breakthrough time for an expanding rice husk fixed bed column decreased from 12.8 to 3.4 h at the increasing flow rate from 5 to 25 ml min^{-1} [31]. Han et al. also reported the breakthrough time reaching saturation has increased dramatically with decrease in flow rate from 10.0 to 5.45 ml min^{-1} [39]. Although the breakthrough time, saturation time and sharpness of the curve was affected by flow rate, the saturation uptake capacity of the column (the amount of metal per unit of adsorbent, mg g^{-1}) was not considerably influenced for Mn(II) (Table 2). It seemed that a high flow rate loaded a large number of metal ions into the column in a very short period of time, resulted in saturation of all the vacant metal-binding sites of the biosorbent. Mainly due to the higher flow

Table 3
Predicted parameters of Bohart–Adams and Wolborska models for the adsorption of Mn(II) by the RHA-packed column

Experimental settings			Bohart–Adams model			Wolborska model	
C_i	F	H	k_{BA}	N_0	r^2	θ_a	r^2
5	10	22.5	20.5×10^{-3}	11.17	0.82	0.23	0.82
10	10	22.5	18.1×10^{-3}	14.37	0.90	0.26	0.90
20	10	22.5	14.9×10^{-3}	23.40	0.96	0.35	0.96
20	5	22.5	6.3×10^{-3}	25.33	0.93	0.16	0.93
20	15	22.5	14.2×10^{-3}	20.30	0.94	0.29	0.94
20	10	7.5	17.7×10^{-3}	19.43	0.93	0.34	0.93
20	10	15.0	15.8×10^{-3}	21.92	0.94	0.35	0.94

Notes: Data in parentheses show standard error of model parameter estimation. C_i = influent metal concentration (mg l^{-1}), F = flow rate (ml min^{-1}), H = Bed height (cm), k_{BA} = Bohart–Adams rate constant ($1 \text{ mg}^{-1} \text{ h}^{-1}$), N_0 = saturation concentration (mg l^{-1}), and θ_a = kinetic coefficient of the external mass transfer (1 h^{-1}).

Table 4
Predicted parameters of Thomas and Yoon–Nelson models for the adsorption of Mn(II) by the RHA-packed column

Experimental settings			Thomas			Yoon–Nelson		
C_i	F	H	k_{TH}	q_0	r^2	K_{YN}	τ	r^2
5	10	22.5	0.035	53.7	0.59	0.18	24.2	0.59
10	10	22.5	0.029	74.2	0.78	0.29	14.4	0.78
20	10	22.5	0.031	93.6	0.87	0.46	14.0	0.87
20	5	22.5	0.010	135.8	0.80	0.19	30.6	0.80
20	15	22.5	0.024	154.8	0.89	0.48	11.6	0.89
20	10	7.5	0.030	252.4	0.90	0.60	9.5	0.90
20	10	15.0	0.017	239.5	0.93	0.35	18.0	0.93

Notes: Data in parentheses show standard error of model parameter estimation. C_i = influent metal concentration (mg l^{-1}), F = flow rate (ml min^{-1}), H = Bed height (cm), k_{TH} = Thomas rate constant ($1 \text{ mg}^{-1} \text{ h}^{-1}$), q_0 = equilibrium metal sorption (mg g^{-1}), k_{YN} = Yoon–Nelson rate constant (1 h^{-1}), τ = the time required for 50% adsorbate breakthrough (h).

rate of metal ions, the residence time of the metal ion in the column was not long enough to obtain the adsorption equilibrium. The metal ions solution might leave the column before the achievement of the equilibrium.

3.5. Modeling of breakthrough curves

The Adams–Bohart and Wolborska models are discussed under the same section of the breakthrough

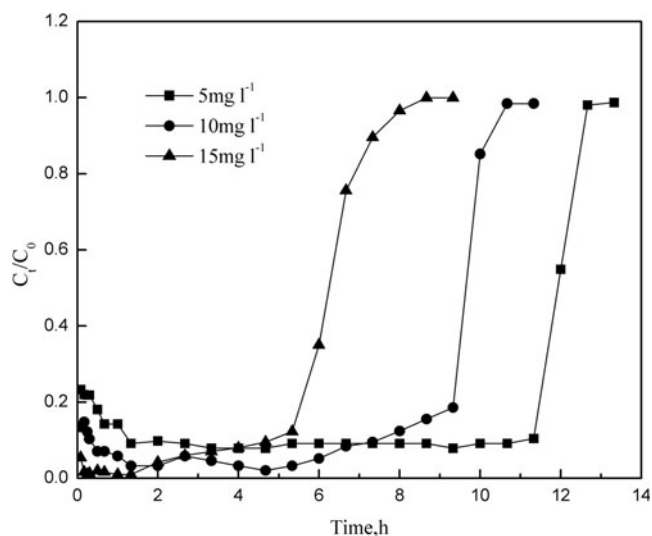


Fig. 2. Experimental breakthrough curves for the adsorption of Mn(II) by the RHA-packed column at different influent metal concentrations.

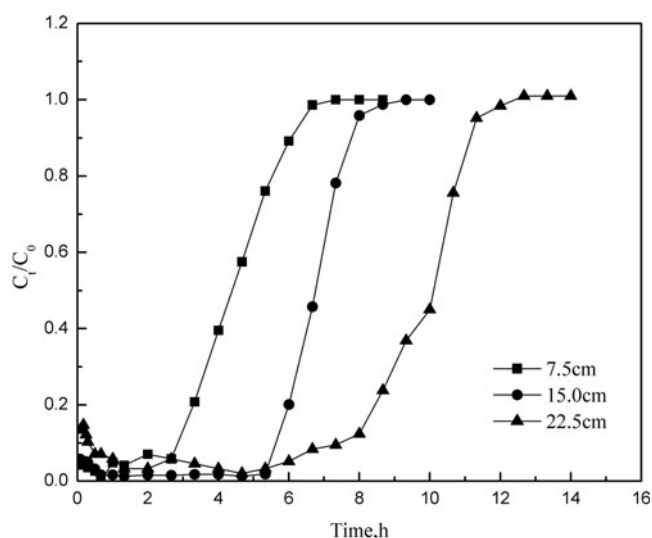


Fig. 3. Experimental breakthrough curves for the adsorption of Mn(II) by the RHA-packed column at different adsorbent dosages.

curves because of the same linear relationship between them and also the direct relation between their constants. A linear relationship between C_t/C_0 and time for various experimental conditions were obtained. In the beginning stages of the experiment, the Bohart–Adams and Wolborska models were fitted to the full part of the breakthrough curves of Figs. 1–3, representing adsorption process of Mn(II) under various experimental conditions. The two models fitted well to

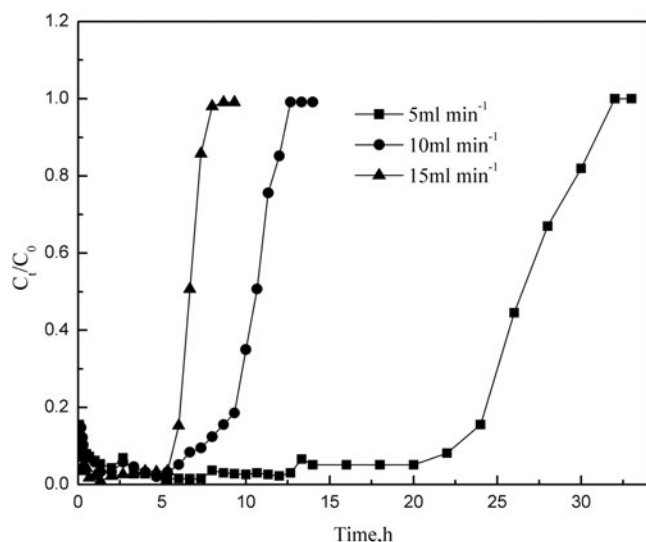


Fig. 4. Experimental breakthrough curves for the adsorption of Mn(II) by the RHA-packed column at different flow rates.

the breakthrough curves ($r^2 > 0.82$) obtained for the adsorption of Mn(II) by the RHA-packed column under different experimental conditions. Respective values of N_0 , k_{AB} and θ_a calculated from the plots of C_t/C_0 vs. time for all experimental conditions are summarized in Table 3 along with corresponding correlation coefficients. Parameters of the two models

suggested some important points regarding column operation. With the increase in the influent Mn(II) concentration and bed height, the saturation concentration (N_0) of column also increased but decreased by increasing flow rate. On contrary, with the increase in the influent Mn(II) concentration and bed height, the saturation concentration (N_0) of column decreased, but increased with the increasing flow rate (Table 3). Therefore, for better saturation concentration (N_0) and kinetic constant (k_{BA}) of the column, influence factors of influent Mn(II) concentration and bed height should be higher, but flow rate needed to reduce. The kinetic coefficient of the external mass transfer (θ_a) of the Wolborska model did not show a precise trend but varied from 0.16 to 0.35, for Mn(II) under various experimental conditions.

The Thomas and Yoon–Nelson models fitted to the breakthrough curves ($r^2 \geq 0.59$) obtained for the adsorption of Mn(II) by the RHA-packed column under different experimental conditions (Table 4). Unlike Bohart–Adams and Wolborska models, these two models fitted well to the breakthrough curves ($r^2 \geq 0.82$) given in Figs. 2–4. These two models showed poor fitness in predicting the breakthrough curves of Mn(II) adsorption by the RHA-packed column. The values of different parameters of the two models were determined using Eqs. (7) and (8) applying the non-linear regression method (Table 4). The Thomas model predicted equilibrium adsorption

Table 5
Adsorption capacities for Mn(II) ions of various adsorbents

Serial no.	Adsorbents	Adsorption capacity (mg/g)	Concentration range (mg/L)	pH	Temp. Range (K)	Refs.
1	Pithacelobium dulce carbon	7.0	5–25	7	–	[40]
2	Manganese oxide coated zeolite	1.1	25–600	6	298	[41]
3	Mesoporous carbons	40	20–200	7	298	[42]
4	Cationic surfactant cetyltrimethyl ammonium bromide-modified mesoporous carbon (CTAB–MC)	43	20–200	7	298	[42]
5	Anionic surfactant sodium dodecyl sulphate-modified mesoporous carbon (SDS–MC)	47	20–200	7	298	[42]
6	Activated carbon from <i>Ziziphus spina-christi</i> seeds	172.41	20–140	4	298–313	[43]
7	Thermally decomposed leaf	66.57	25–1,200	7.3	278–328	[44]
8	<i>Pseudomonas</i> sp.	109	50–500	6	288–318	[45]
9	Crab shell particles	69.9	10–1,000	6	296	[46]
10	Rice husk ash	7.57	5–20	6	298	Present study

Mn(II)

quantity, q_0 , was higher at higher influent Mn(II) concentration, longer bed height and lower flow rates. However, the Thomas kinetic constant was usually higher at lower influent Mn(II) concentration, lower bed height and higher flow rate. The Yoon–Nelson model rate constant generally increased with increasing influent metal concentration and flow rate, but it decreased with increasing bed height. The Yoon–Nelson constant, value of τ , expressing the time required for 50% breakthrough, decreased with increasing influent metal concentration and flow rates, nevertheless, increased with increasing bed height. The value of τ calculated from the model equation better matched the experimental data of various experimental conditions (Figs. 2–4 and Table 4). However, as Thomas and Yoon–Nelson models showed a low fit to the experimental data, so these two models were considered as unsuitable kinetic models to describe Mn(II) adsorption in a fixed bed of RHA.

3.6. Comparison study

The maximum amount of Mn(II) ions from aqueous solutions onto RHA was compared with other adsorbents reported in literature was present in Table 5. It can be seen that maximum adsorptive capacities for Mn(II) ions were different for various materials used. Metal ion concentration, pH, and temperature have a certain influence on the adsorption capacity.

4. Conclusions

RHA-packed column showed promising capability of adsorbing metal ions from aqueous systems. Breakthrough and saturation time of the column largely depended on influent Mn(II) concentration, flow rate and bed height. Saturation time of the column was longer when Mn(II) concentration and flow rate were lower, but the higher the bed height, the longer the running time. The maximum adsorption percentage was 96.59 when Mn(II) concentration was 5 mg L^{-1} , flow rate was 10 mL min^{-1} and the bed height was 22.5 cm. Bohart–Adams and Wolborska models were found to be the most suitable to estimate breakthrough curves obtained under varying experimental conditions. As other adsorbents, RHA need recycle. RHA is an effective and alternative material for the removal of Mn(II) ions from waste water because of its high biosorption capacity, abundant availability and cost-effectiveness. So it could be used to removal other heavy metal ions in the future. Future research should focus on the adsorption characteristics of the coexistence of multiple ions condition.

Acknowledgement

This study was supported by the National Scientific and Technological Supporting Project, China (2013BAJ12B01).

References

- [1] D. Park, Y.S. Yun, J.H. Jo, J.M. Park, Biosorption process for treatment of electroplating wastewater containing Cr(VI): Laboratory-scale feasibility test, *Ind. Eng. Chem. Res.* 45 (2006) 5059–5065.
- [2] F.W. Pontius, *Water Quality and Treatment*, fourth ed., McGraw-Hill Inc, New York, NY, 1990.
- [3] K.S. Low, C.K. Lee, S.C. Liew, Sorption of cadmium and lead from aqueous solutions by spent grain, *Process Biochem.* 36 (2000) 59–64.
- [4] S.E. Bailey, T.J. Olin, R.M. Bricka, D.D. Adrian, A review of potentially low-cost sorbents for heavy metals, *Water Res.* 33 (1999) 2469–2479.
- [5] M. Zaw, B. Chiswell, Iron and manganese dynamics in lake water, *Water Res.* 33 (1999) 1900–1910.
- [6] C.L. Keen, S. Zidenberg-Cherr. Manganese toxicity in humans and experimental animals, in: D.J. Klimis-Tavantzis, *Manganese in Health and Disease*, ed., CRC Press, Boca Raton, LA, (1994), pp. 194–205.
- [7] P. Nyberg, P. Andersson, E. Degerman, H. Borg, E. Olofsson, Labile inorganic manganese? An overlooked reason for fish mortality in acidified streams? *Water Air Soil Pollut.* 85 (1995) 333–340.
- [8] L.I. Sly, M.C. Hodgkinson, V. Arunpairojana, Deposition of manganese in a drinking water distribution system, *Appl. Environ. Microbiol.* 56 (1990) 628–639.
- [9] K.V. Heal, P.E. Kneale A.T. Donald, Manganese mobilization and runoff process in upland catchments, in: *British Hydrological Society 5th National hydrology, Symposium, Edinburgh, 1995*, pp. 911–918.
- [10] D. Ellis, C. Bouchard, G. Lantagne, Removal of iron and manganese from groundwater by oxidation and microfiltration, *Desalination* 130 (2000) 255–264.
- [11] A. Kumar, N.N. Rao, S.N. Kaul, Alkali-treated straw and insoluble straw xanthate as low cost adsorbents for heavy metal removal-preparation, characterization and application, *Bioresour. Technol.* 71 (2000) 133–142.
- [12] P. Kumar, S.S. Dara, Binding heavy metal ions with polymerized onion skin, *J. Polym. Sci Polym. Chem.* 19 (1981) 397–402.
- [13] N.T. Abdel-Ghani, M. Hefny, G.A.F. El-Chaghaby, Removal of lead from aqueous solution using low cost abundantly available adsorbents, *Int. J. Environ. Sci. Technol.* 4 (2007) 67–73.
- [14] K.K. Singh, R. Rastogi, S.H. Hasan, Removal of Cr(VI) from wastewater using rice bran, *J. Colloid Interface Sci.* 290 (2005) 61–68.
- [15] A. Saeed, M.W. Akhter, M. Iqbal, Removal and recovery of heavy metals from aqueous solution using papaya wood as a new biosorbent, *Sep. Purif. Technol.* 45 (2005) 25–31.
- [16] M. Ghorbani, H. Eisazadeh, Fixed bed column study for Zn, Cu, Fe and Mn removal from wastewater using nanometer size polypyrrole coated on rice husk ash, *Synthetic Met.* 162 (2012) 1429–1433.

- [17] D.P. Tiwari, D.K. Singh, D.N. Saksena, Hg(II) adsorption from aqueous solutions using rice-husk ash, *J. Environ. Eng.* 121 (1995) 479–481.
- [18] Q. Feng, Q. Lin, F. Gong, S. Sugita, M. Shoya, Adsorption of lead and mercury by rice husk ash, *J. Colloid Interface Sci.* 278 (2004) 1–8.
- [19] V.C. Srivastava, I.D. Mall, I.M. Mishra, Equilibrium modeling of ternary adsorption of metal ions onto rice husk ash, *J. Chem. Eng. Data* 54 (2009) 705–711.
- [20] S. Ayoob, A.K. Gupta, P.B. Bhakat, Analysis of breakthrough developments and modeling of fixed bed adsorption system for As(V) removal from water by modified calcined bauxite (MCB), *Sep. Purif. Technol.* 52 (2007) 430–438.
- [21] P.B. Bhakat, A.K. Gupta, S. Ayoob, Feasibility analysis of As(III) removal in a continuous flow fixed bed system by modified calcined bauxite (MCB), *J. Hazard. Mater.* 139 (2007) 286–292.
- [22] S.K. Maji, A. Pal, T. Pal, A. Adak, Modeling and fixed bed column adsorption of As(III) on laterite soil, *Sep. Purif. Technol.* 56 (2007) 284–290.
- [23] R. Han, D. Ding, Y. Xu, W. Zou, Y. Wang, Y. Li, L. Zou, Use of rice husk for the adsorption of congo red from aqueous solution in column mode, *Bioresour. Technol.* 99 (2008) 2938–2946.
- [24] V.C. Srivastava, I.D. Mall, I.M. Mishra, Removal of cadmium(II) and zinc(II) metal ions from binary aqueous solution by rice husk ash, *Colloids Surf., A: Physicochem. Eng. Aspects* 312 (2008) 172–184.
- [25] F. Ji, C. Li, J. Xu, P. Liu, Dynamic adsorption of Cu(II) from aqueous solution by zeolite/cellulose acetate blend fiber in fixed-bed, *Colloids Surf., A: Physicochem. Eng. Aspects* 434 (2013) 88–94.
- [26] M. Ghasemi, A.R. Keshtkar, R. Dabbagh, S. Jaber Safdari, Biosorption of uranium(VI) from aqueous solutions by Ca-pretreated *Cystoseira indica* alga: Breakthrough curves studies and modeling, *J. Hazard. Mater.* 189 (2011) 141–149.
- [27] O. Hamdaoui, Dynamic sorption of methylene blue by cedar sawdust and crushed brick in fixed bed columns, *J. Hazard. Mater.* 138 (2006) 293–303.
- [28] J. Goel, K. Kadirvelu, C. Rajagopal, V. Kumar Garg, Removal of lead(II) by adsorption using treated granular activated carbon: Batch and column studies, *J. Hazard. Mater.* 125 (2005) 211–220.
- [29] M. Zendejdel, A. Barati, H. Alikhani, Removal of heavy metals from aqueous solution by poly(acrylamide-co-acrylic acid) modified with porous materials, *Polym. Bull.* 67 (2011) 343–360.
- [30] R. Ashkenazy, L. Gottlieb, S. Yannai, Characterization of acetone-washed yeast biomass functional groups involved in lead biosorption, *Biotechnol. Bioeng.* 55 (1997) 1–10.
- [31] X. Luo, Z. Deng, X. Lin, C. Zhang, Fixed-bed column study for Cu²⁺ removal from solution using expanding rice husk, *J. Hazard. Mater.* 187 (2011) 182–189.
- [32] S. Sugashini, K.M.M.S. Begum, Performance of ozone treated rice husk carbon (OTRHC) for continuous adsorption of Cr (VI) ions from synthetic effluent, *J. Environ. Chem. Eng.* 1 (2013) 79–85.
- [33] P. Lodeiro, R. Herrero, M.E. Vicente, The use of protonated *Sargassum muticum* as biosorbent for cadmium removal in a fixed-bed column, *J. Hazard. Mater.* 137 (2006) 244–253.
- [34] M.C. Fournier-Salaün, P. Salaün, Quantitative determination of hexavalent chromium in aqueous solutions by UV-Vis spectrophotometer, *Cent. Eur. J. Chem.* 5 (2007) 1084–1093.
- [35] N.K.E.M. Yahaya, I. Abustan, M.F.P.M. Latiff, O.S. Bello, M.A. Ahmad, Fixed-bed column study for Cu (II) removal from aqueous solutions using rice husk based activated carbon, *Int. J. Eng. Technol.* 11 (2011) 248–252.
- [36] K. Vijayaraghavan, J. Jegan, K. Palanivelu, M. Velan, Batch and column removal of copper from aqueous solution using a brown marine alga *Turbinaria ornata*, *Chem. Eng. J.* 106 (2005) 177–184.
- [37] Z. Aksu, G. Eğretli, T.A. Kutsal, A comparative study of copper(II) biosorption on Ca-alginate, agarose and immobilized *C. vulgaris* in a packed-bed column, *Process Biochem.* 33 (1998) 393–400.
- [38] S. Sugashini, K.M.M.S. Begum, Performance of ozone treated rice husk carbon (OTRHC) for continuous adsorption of Cr (VI) ions from synthetic effluent, *J. Environ. Chem. Eng.* 1 (2013) 79–85.
- [39] R. Han, W. Zou, H. Li, Y. Li, J. Shi, Copper(II) and lead(II) removal from aqueous solution in fixed-bed columns by manganese oxide coated zeolite, *J. Hazard. Mater.* 137 (2006) 934–942.
- [40] K.A. Emmanuel, A.V. Rao, Adsorption of Mn(II) from aqueous solutions using pithacelobium dulce carbon, *Rasayan J. Chem.* 1 (2008) 840–852.
- [41] S.R. Taffarel, J. Rubio, Removal of Mn²⁺ from aqueous solution by manganese oxide coated zeolite, *Miner. Eng.* 23 (2010) 1131–1138.
- [42] M. Anbia, S. Amirmahmoodi, Removal of Hg(II) and Mn (II) from aqueous solution using nanoporous carbon impregnated with surfactants, *Arab. J. Chem.* 2011. Available from: <http://dx.doi.org/10.1016/j.arabjc.2011.04.004>.
- [43] A. Omri, M. Benzina, Removal of manganese(II) ions from aqueous solutions by adsorption on activated carbon derived a new precursor: *Ziziphus spina-christi* seeds, *Alexandria Eng. J.* 51 (2012) 343–350.
- [44] Z.Z. Li, S. Imaizumi, T. Katsumi, T. Inui, X.W. Tang, Q. Tang, Manganese removal from aqueous solution using a thermally decomposed leaf, *J. Hazard. Mater.* 177 (2010) 501–507.
- [45] D. Gialamouidis, M. Mitrakas, M. Liakopoulou-Kyriakides, Equilibrium, thermodynamic and kinetic studies on biosorption of Mn(II) from aqueous solution by *Pseudomonas* sp., *Staphylococcus xylosus* and *Blakeslea trispora* cells, *J. Hazard. Mater.* 182 (2010) 672–680.
- [46] K. Vijayaraghavan, H.Y.N. Winnie, R. Balasubramanian, Biosorption characteristics of crab shell particles for the removal of manganese(II) and zinc(II) from aqueous solutions, *Desalination* 266 (2011) 195–200.